Journal of Alloys and Compounds 642 (2015) 166–171

Contents lists available at ScienceDirect

Journal of Alloys and Compounds

journal homepage: www.elsevier.com/locate/jalcom

Letter

Leakage properties of $BaTiO_3$ thin films on polycrystalline Ni substrates grown by polymer-assisted deposition with two-step annealing

Hui Du [a,b], Weizheng Liang [a], Yang Li [a], Min Gao [a], Yin Zhang [a], Chonglin Chen [c,d], Yuan Lin [a,b,*]

[a] State Key Laboratory of Electronic Thin films and Integrated Devices, University of Electronic Science and Technology of China, Chengdu, Sichuan 610054, PR China
[b] Institute of Electronic and Information Engineering in Dongguan, University of Electronic Science and Technology of China, Dongguan, Guangdong 523808, PR China
[c] Department of Physics and Astronomy, University of Texas at San Antonio, San Antonio, TX 78249, USA
[d] Department of Physics and the Texas Center for Superconductivity, University of Houston, Houston, TX 77204, USA

ARTICLE INFO

Article history:
Received 29 January 2015
Received in revised form 24 March 2015
Accepted 5 April 2015
Available online 9 April 2015

Keywords:
Polymer-assisted deposition
Rapid thermal annealing
$BaTiO_3$
Leakage current

ABSTRACT

Ferroelectric $BaTiO_3$ (BTO) thin films were successfully deposited on nickel substrates by a chemical solution deposition technique named polymer-assisted deposition. A NiO_x buffer layer and a first annealing in a reducing environment were adopted to control the interdiffusion and oxidation of the substrates. It was found that a second annealing in oxygen using a rapid thermal annealing furnace would strongly affect the electrical properties of the BTO thin films, especially the leakage current density. The leakage current density with the optimized annealing condition can be reduced by about two orders of magnitude. The correlation between the second annealing conditions and leakage current densities was established. Mechanisms of the leakage and impacts from the oxygen vacancies and interface evolution have been discussed.

1. Introduction

Ferroelectric oxide thin films have been investigated for many years and have shown great potential in many applications due to their excellent ferroelectric, dielectric and piezoelectric properties [1–8]. Previous research on ferroelectric oxide thin films was usually conducted on oxide substrates (such as $SrTiO_3$ and $LaAlO_3$), or Si substrates coated with noble-metal (such as Pt and Au). In the last two decades, ferroelectric oxide thin films grown directly on the surfaces of base-metallic substrates have been considered for promising applications in structural health monitoring systems, embedded capacitors, super-capacitors and MEMS [9–18]. Compared to oxide substrates and noble-metal coated substrates, the base-metallic substrates such as nickel and copper, which take the advantage of low cost, are much easier to get oxidized. On one side, to avoid the serious oxidation of the base-metallic substrates, high temperature synthesis of the ferroelectric oxide films should be performed in a reducing ambient. On the other side, to ensure the oxygen content in the ferroelectric oxide thin films, a proper source of oxygen needs to be provided during the process. Moreover, the diffusion at the interface between the ferroelectric oxide thin film and the base-metallic substrate needs to be well controlled.

Facing these challenges, several groups have initiated the efforts to grow ferroelectric oxide thin films on base-metallic substrates such as Ni foils by a variety of techniques, including pulsed laser deposition (PLD) [14–16], sputtering [17–19], and chemical solution deposition (CSD) [11–13]. In our previous research, we have demonstrated the feasibility of using a CSD technique called polymer-assisted deposition (PAD) to synthesize ferroelectric $BaTiO_3$ (BTO) thin films on polycrystalline Ni substrates [20–22]. The major distinction between this PAD process and other chemical solution techniques is that a soluble polymer plays a significant role in preparing a stable and homogeneous solution by binding the metal ions with the polymer in the PAD process [23]. No hydrolysis reaction is required. Thus, the stability of the precursor solution and the controllability of the process can be greatly improved [23]. Our previous investigations have indicated that a NiO_x buffer layer prepared by a pretreatment of the Ni foils in H_2O_2 solutions is crucial in achieving a good dielectric performance of the as-prepared BTO thin films on Ni foils [20–22]. The NiO_x layer serves not only as a buffer layer to suppress interdiffusion but also as an oxygen source for the synthesis of BTO film [21]. However, since the BTO films were annealed in the reducing ambient at high temperature for a long time, it is quite possible that oxygen vacancies may still exist in the films. A second annealing

* Corresponding author at: State Key Laboratory of Electronic Thin films and Integrated Devices, University of Electronic Science and Technology of China, Chengdu, Sichuan 610054, PR China. Tel.: +86 28 83208813.
E-mail address: linyuan@uestc.edu.cn (Y. Lin).

http://dx.doi.org/10.1016/j.jallcom.2015.04.025
0925-8388/

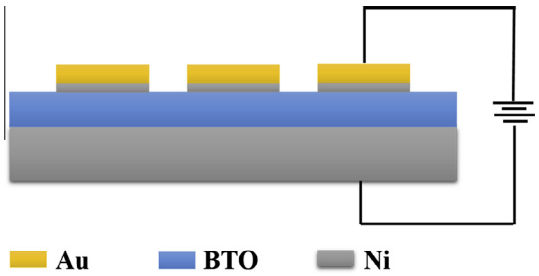

Fig. 1. Schematic diagram of the test structure.

may be helpful to compensate these oxygen vacancies which would strongly impact the leakage current.

Thus, this paper presents our effort to further improve the leakage performance of the BTO films on polycrystalline Ni foils grown by PAD through a second annealing process in air. The correlation between annealing conditions and leakage properties of the films will be discussed. Leakage mechanisms of the films under various annealing conditions will be analyzed.

2. Experimental

Firstly, precursor solutions containing Ba^{2+} and Ti^{4+} ions were prepared as previously reported [21]. Then, the Ba^{2+} and Ti^{4+} precursor solutions were mixed in a molar ratio of 1:1 to yield a homogonous precursor solution. Commercial polycrystalline nickel foils (99.9%) with the thickness of 0.5 mm were mechanically polished and ultrasonically cleaned in acetone to remove the natural oxide layers and surface contaminations. Then, the foils were immersed into 10% hydrogen peroxide (H_2O_2) solution at 50 °C for 2 h to form nickel oxide layers. This pretreatment has been proved to be crucial to achieve BTO thin films with good performance [20,21].

The as-prepared precursor solution was spin-coated on the pretreated nickel foils with a spin rate of 3000 rpm for 30 s. The wet precursor films were then put into a tube furnace for heat treatment. To decompose the polymer, the precursor films were first heated to 510 °C slowly and stayed at that temperature for 1 h. To yield a 500-nm-thick film, the spin coating and the above thermal treatment process need to be repeated for 5 times. Then, the films were further heated up to 800 °C and stayed there for 30 min for the crystallization of BTO, before being cooled down slowly to room temperature. It should be noted that a forming gas containing 94% N_2 and 6% H_2 with a flow rate of 100 mL/min was chosen as the ambient during the whole heat treatment process, in which the oxygen partial pressure is about 10^{-18} atm.

In order to further compensate the oxygen vacancies in BTO thin film, a second annealing process in air using a rapid-thermal annealing (RTA) furnace was conducted on the as-prepared samples. The reason to use the RTA furnace is to reduce the thermal exposure of the samples at the temperature where Ni is easily oxidized. Thus, the as-prepared samples were heated in air in the RTA furnace from room temperature to 400 °C in 80 s. Then the samples stayed there for a certain period of time to absorb oxygen before being cooled down. To find out the optimized condition for the post annealing, the annealing time at 400 °C, named as RTA time in this paper, varied from 30 to 120 min. For comparison, a reference sample without the RTA process was also prepared.

The crystallinity of the films was examined by the X-ray diffraction (XRD) technique. A 200-nm-thick Au layer and an underneath 10-nm-thick Ni adhesive layer were deposited by sputtering at room temperature on the surface of BTO film as the top electrode. The area of the electrode is about 4×10^{-4} cm^2. Electrical measurements were all performed on a home-made probe station in which the diameter of each tip is less than 20 μm. Dielectric properties of the samples were tested using an Agilent-4284A precision LCR meter. Leakage currents were measured using a Keithley 2400 source meter. Voltage was applied as schematically shown in Fig. 1. The applied voltage varied from −10 V to 0 V, and then from 0 V to +10 V.

3. Results and discussions

Fig. 2 shows the XRD θ–2θ scanning patterns for samples with different RTA time. No significant difference can be observed between the reference sample (labeled as 0 min) and the samples post-annealed by RTA, suggesting that the crystalline phases of all the BTO films are similar. All the peaks in the patterns can be indexed as the perovskite BTO and polycrystalline Ni. The intensities of the BTO diffraction peaks indicate that the BTO films have no preferred orientation. Lattice parameters of the BTO films can be

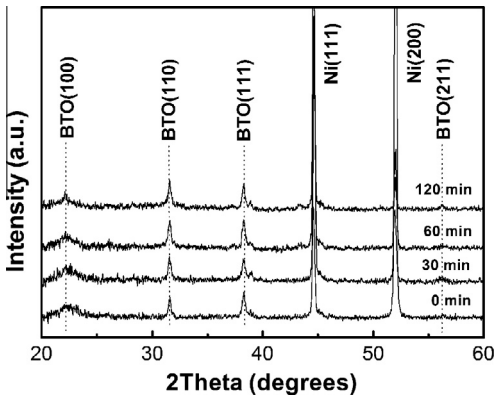

Fig. 2. XRD θ–2θ scanning patterns of BTO thin films on Ni substrates with different RTA time.

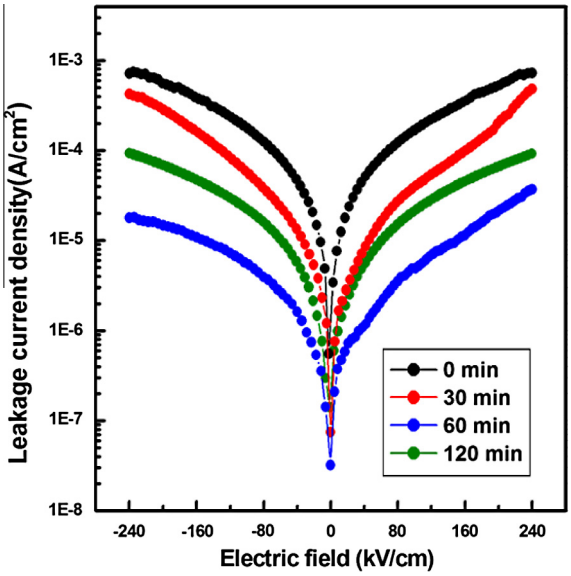

Fig. 3. Variation of the leakage current density with the applied electric field for the samples with different RTA time.

calculated based on the XRD data, which are $a = 3.99$ Å, $b = 4.04$ Å, and $c = 4.12$ Å. The values are very close to those of the bulk perovskite BTO, suggesting that the BTO thin films have been successfully fabricated with a pure polycrystalline perovskite phase. Moreover, no NiO or Ni_2O_3 peak has been detected, implying that the RTA treatment did not induce the crystalline nickel oxide layers thick enough to be detected by XRD.

The leakage current densities were measured for the BTO thin films treated by RTA as well as the reference sample. The results are plotted in Fig. 3. It is shown that the leakage current density has been effectively suppressed basically after the second annealing in the RTA furnace. The leakage current density could be reduced by about two orders of magnitude when the RTA time increases from 0 to 60 min. For the as-prepared BTO thin films, oxygen vacancies might be the key source for the leakage current [24–31]. The second annealing process is in fact a process in which the BTO thin films absorb oxygen from the air and compensate the oxygen vacancies. Thus, the leakage current density can be suppressed. However, it is also indicated that when the second annealing time further increased from 60 to 120 min, the leakage current density increased again. The reason may lie in the change of the interface which strongly impacts the leakage mechanisms in the BTO film.

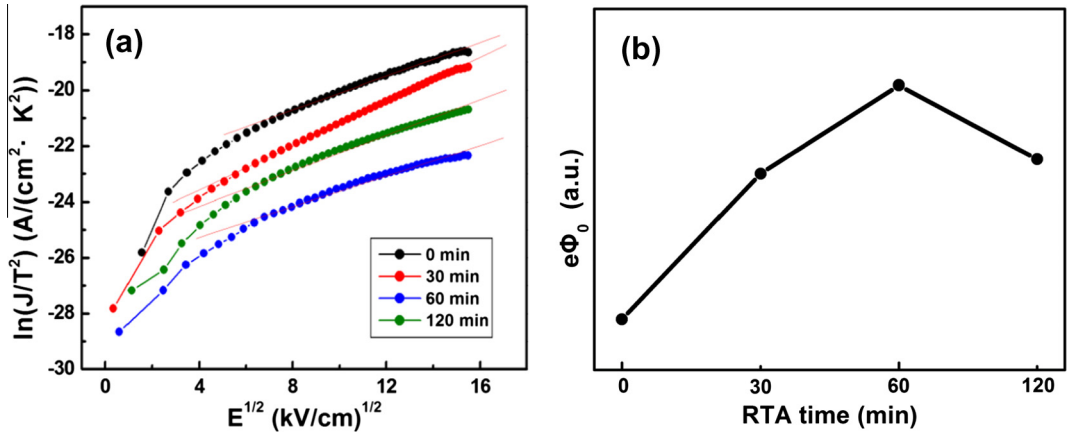

Fig. 4. Plots of $\ln(J/T^2)$ versus $E^{1/2}$ for the leakage current density data measured under the negative bias (a) and the estimated Schottky barrier height (b) for BTO thin films with different RTA time.

Leakage mechanisms of ferroelectric thin films on various single crystal substrates have been discussed intensively in literatures [25,26,28]. However, a clear understanding is yet to be made for this special structure of BTO/Ni fabricated by PAD. Thus, the leakage current densities of the BTO thin films measured under different voltages were analyzed in details to understand the leakage mechanisms. When the applied electric field was low (<50 kV/cm), the plot of the current density (J) versus the applied electric field (E) exhibits a linear relationship with the slope of about 1. Thus, the leakage current belongs to Ohmic conductive mechanism, which can be expressed as:

$$J = n_0 e E \mu = \frac{n_0 e \mu V}{d} \tag{1}$$

where n_0 is the carrier density, e is the elementary charge, μ is the carrier mobility, V is the applied voltage, and d is the thickness of the thin film. This phenomenon occurred probably due to that intrinsic carriers exist in the crystal grains, the number of which meets the requirement of the ohmic conductive mechanism when the voltage is low enough.

With the increase of the applied electric field, different leakage mechanisms may occur and become dominant. When the Au electrode is under a negative bias voltage, the leakage current flows from the bottom Ni substrate to the top Au electrode. From the plots of $\ln(J/T^2)$ versus $E^{1/2}$ shown in Fig. 4(a), it can be seen that all plots fit well as a linear relationship. This implies that the Schottky emission mechanism may exist when the electric field is higher than 50 kV/cm. The Schottky emission mechanism can be expressed as:

$$J = A^* T^2 \exp\left[\frac{-e\left(\phi_0 - \sqrt{eE/4\pi\varepsilon_i\varepsilon_0}\right)}{kT}\right] \tag{2}$$

where ε_0 is the permittivity of free space, ε_i is the optical dielectric constant, A^* is the Richardson constant, T is the absolute temperature, k is the Boltzmann constant, and $e\ \phi_0$ is the Schottky barrier height.

The data suggests that there is a surface Schottky barrier between the Au electrode (with the underneath Ni adhesive layer) and the BTO thin film. When the electric field is high enough, the electrons penetrated into the BTO thin film through the Schottky electronic tunneling.

From the slopes of the plots in Fig. 4(a), the optical dielectric constant ε_i can be calculated, which are 2.11, 1.38, 3.05 and 2.22 when the RTA time periods are 0 min, 30 min, 60 min and 120 min, respectively. The values are all smaller than the reported optical dielectric constant of about 5 for BTO bulk [17]. The results, on one hand may come from the different quality of our BTO thin film samples with the reported bulks, on the other hand may imply other conductive mechanisms co-existing in the films.

From the intercept values of the plots in Fig. 4(a), we can estimate the trend of change in the Schottky barrier height ($e\ \phi_0$) with the RTA time, as shown in Fig. 4(b). When the RTA time increases from 0 to 60 min, the Schottky barrier height increases, and the highest value appears when RTA time is 60 min. However, the Schottky barrier height decreases when the RTA time further increases from 60 to 120 min. The variation trend of the Schottky barrier height directly indicates the evolution of the interface between the Au/Ni electrode and the BTO thin film. It is easy to understand that a Schottky barrier would be formed between the BTO film and the Ni adhesive layer underneath the Au electrode since the adhesive and electrode layers were deposited by sputtering at room temperature. As the BTO thin films were firstly annealed in the reducing ambient at high temperature (~800 °C) for 30 min, oxygen vacancies should unavoidably exist in the films, especially near the top surface of the BTO thin films. The oxygen vacancies on the top surface would induce a relatively low Schottky barrier height [32], which is the case of the reference sample. When a second annealing was performed in oxygen, the oxygen diffused into the films and compensated the oxygen vacancies, especially at the surface, which would increase the Schottky barrier height. This could be the scenario when the RTA time increases from 0 to 60 min. On the other hand, interdiffusion between the Ni substrates and the BTO thin films would also happen during the second annealing. Thus, when the RTA time is longer than the optimized length (60 min as indicated by current experiments), the Schottky barrier height would decrease due to the diffusion of Ni into BTO films, which may be the case of the sample with RTA time of 120 min.

Moreover, since the oxygen vacancies may exist not only at the surface but also throughout the BTO thin film, other conductive mechanisms such as Frenkel–Poole (F–P) emission mechanism and space charge limited current (SCLC) mechanism also need to be checked.

The F–P emission mechanism can be expressed as:

$$J = CE \exp\left[\frac{-e\left(\phi_t - \sqrt{eE/\pi\varepsilon_i\varepsilon_0}\right)}{kT}\right] \tag{3}$$

where C represents a constant and ϕ_t is the trapped barrier height. When we plotted $\ln(J/E)$ versus $E^{1/2}$ from the data in the range of the negative bias in Fig. 3, we found that all the plots fit well with a

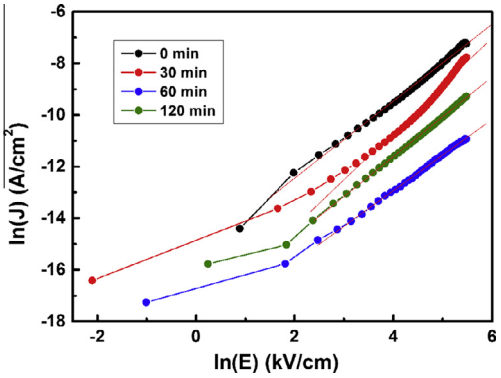

Fig. 5. Plots of ln(J) versus ln(E) for the leakage current density data measured under the negative bias for BTO thin films with different RTA time.

linear relationship. However, the optical dielectric constants calculated from the slopes of the plots are about one order of magnitude higher than the reported value of 5. This suggested F–P emission may not act as the key roles in the leakage mechanisms under this measurement condition.

The SCLC mechanism follows the equation of:

$$J = \frac{9}{8}\varepsilon_r\varepsilon_0\mu\frac{V^2}{d^3} = \frac{9}{8}\varepsilon_r\varepsilon_0\mu\frac{E^2}{d} \quad (4)$$

where ε_r is the low frequency dielectric constant.

Fig. 5 shows the plots of ln(J) versus ln(E) based on the data in the range of the negative bias in Fig. 3. The slopes of the plots are 1.54, 1.88, 1.36 and 1.55 for the samples with RTA time of 0 min, 30 min, 60 min and 120 min, respectively. The values are close to 2, implying that the SCLC mechanism may also play one of the key roles.

Given that the BTO films were originally sintered in reducing atmosphere, we assume that oxygen vacancies exist in the BTO thin films. The oxygen vacancies are believed to be related to the origin of the space charges in many ferroelectric materials [32–35]. Moreover, two pathways for the movement of oxygen need to be noticed during the first annealing. On one hand, the oxygen diffuses into the BTO films from the interfacial NiO_x layers because the free energy of BTO (−1854 kJ/mol, at 1100 K) is much lower than NiO (−315 kJ/mol, at 1100 K) [21,36]. On the other hand, oxygen loses from the surface of the BTO thin film in reducing ambient at high temperature. Thus, a gradient distribution of oxygen vacancies across the thickness of the BTO thin films would be formed, which would contribute to the formation of the space charge region under the electric field. Normally, oxygen vacancies are donor-like trapping centers for electrons, whose energy levels are very close to the conduction band and are readily to activate electrons to be mobile. The less oxygen vacancies there are, the less free carriers the films can generate, hence a lower conductivity would occur. That is why the leakage current reduces when the RTA time increases from 0 to 60 min. However, with a further increase of the RTA time, the diffusion of Ni from the substrates could not be negligible. It has been demonstrated by Qi, et al. that the dominant charge compensation mechanism in the Ni^{2+} doped $BiFeO_3$ is the creation of oxygen vacancies [35]. As a result, the leakage current would increase again, which is the case of the sample with the RTA time of 120 min.

Thus, both the Schottky emission and SCLC may play important roles as the leakage mechanisms in the BTO film under the negative bias. It is interesting to note that the bigger the difference of the optical dielectric constant deduced from Schottky emission mechanism with the reported bulk value, the closer the slope of the SCLC fitting curve is to the value of 2, which may imply the coexistence and competition of the two conduction mechanisms in the thin films.

When Au electrode is under a positive bias voltage, leakage current flows from the top Au electrode to the bottom Ni substrate. Similarly, when the electric field is very low, the J–E curve fits well with the Ohmic conductive mechanism. When the electric field increases to a higher level, other mechanisms occur.

The Ni substrates have been pretreated in the H_2O_2 solutions and thus a NiO_x buffer layer has been formed before the BTO deposition. However, as demonstrated in our previous publications, during the first time annealing process of BTO in the reducing ambient, this NiO_x layer serves as not only the buffer layer to suppress the interdiffusion between the Ni and BTO but also the oxygen source since the BTO can deprive oxygen from this layer [21]. And under the optimized condition (2 h pretreatment) which was used in this experiment, the NiO_x layer should be reduced into a Ni nanocrystalline layer. Our previous results also demonstrated that the interdiffusion of oxygen and Ni introduced an Ohmic contact at the interface of BTO thin films and the Ni substrates [37]. This argument was supported by plotting the ln(J/T^2) versus $E^{1/2}$ under the positive bias (not shown here) based on the data from Fig. 3, which does not exhibit a good linear relationship for any of the samples, suggesting that Schottky emission does not dominate the conduction mechanism in this case.

Plots of ln(J) versus ln(E) were fit to check the SCLC mechanism. Interestingly, linear relationship with the slopes of 1.45, 1.98, and 1.56 are observed for samples with RTA time periods of 0 min,

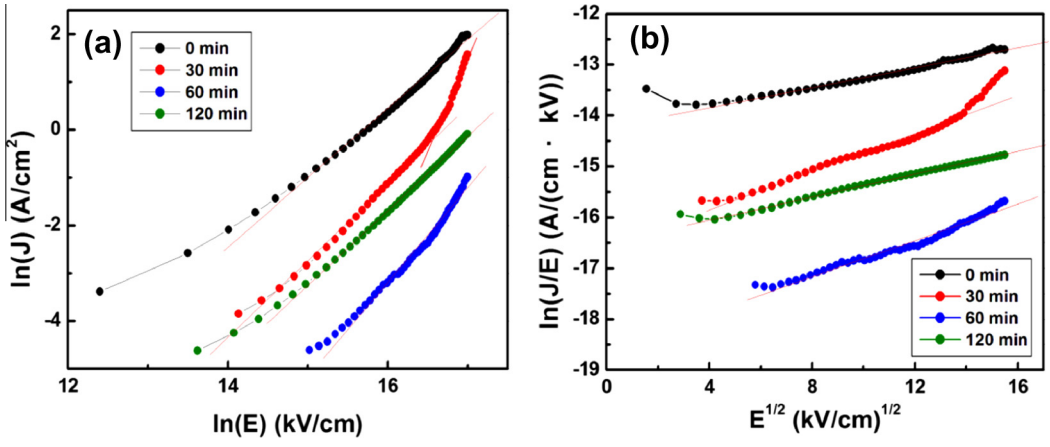

Fig. 6. Plots of ln(J) versus ln(E) (a) and ln(J/E) versus $E^{1/2}$ (b) for the leakage current density data measured under the positive bias for BTO thin films with different RTA time.

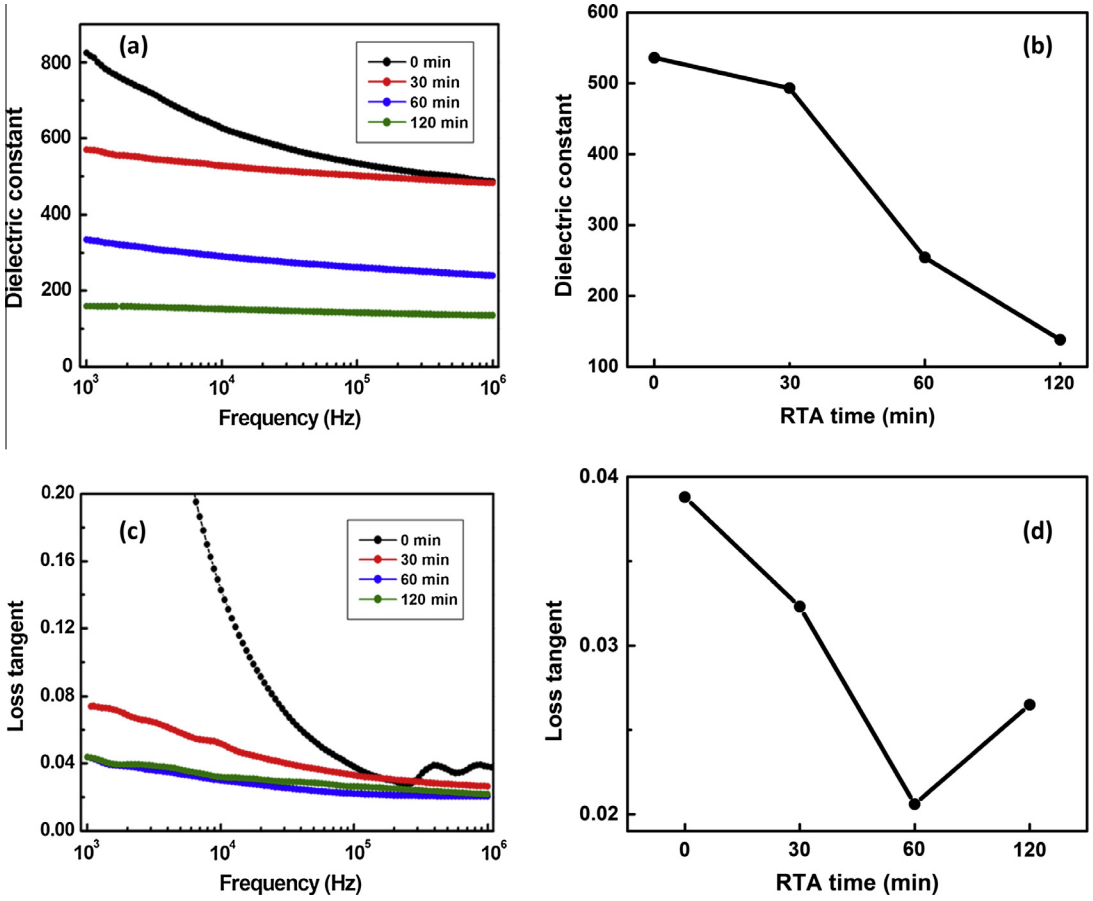

Fig. 7. Dielectric constant versus the frequency (a), dielectric constant at 100 kHz and zero applied electric field (b), loss tangent versus the frequency (c), and loss tangent at 100 kHz and zero applied electric field (d) for BTO samples with different RTA time.

60 min and 120 min, respectively (as shown in Fig. 6(a)). The results show that the SCLC dominates the leakage mechanism in the samples. And for the sample with RTA time of 30 min, the plot can be divided into two linear parts with the slopes of 1.61 and 3.96 for the lower field and the higher field, respectively. This suggests that there might be different types of defects in this sample, which belong to discrete energy levels [38–41]. The phenomenon may be attributed to the defects created during the sample fabrication process. Then the defect-related discrete energy levels appeared in the forbidden band. The energy level influenced carriers transport and conductive emission strongly. More research is needed in the future to find out the reason that this phenomenon does not appear in the other samples with different RTA time.

Manifest linear relation of $\ln(J/E)$ versus $E^{1/2}$ can be observed for all the samples except at the high electric field range for the sample with the RTA time of 30 min (as shown in Fig. 6(b)). However, similar to the case under the negative bias, the optical dielectric constants calculated from the slope of the plots are about one order of magnitude higher than the reported value of 5, indicating that the F–P emission may not act as the key role in the leakage mechanisms under this measurement condition.

Dielectric constant and loss tangent were measured for each sample at the frequency range from 0 to 10^6 Hz as shown in Fig. 7(a) and (c). The results at 100 kHz versus the RTA treated time of the BTO thin films were plotted in Fig. 7(b) and (d), respectively. It is clearly indicated that the samples treated by RTA exhibit reduction in dielectric loss compared to the reference sample. The BTO thin film treated by RTA for 60 min exhibits the lowest dielectric loss tangent of 0.02 at 100 kHz, about a 47% decrease compared to the reference sample. The compensation of oxygen vacancies in the BTO thin films during the second annealing should account for the reduction of the overall dielectric loss. It should be also noticed that the dielectric constant deceases with the increase of the RTA time. As discussed above, the increase of Schottky barrier height with the RTA time and the degradation of dielectric properties due to the interdiffusion between the BTO films and the Ni substrates after long time annealing should be the key reasons for the decrease of the dielectric constant with the RTA time.

4. Conclusions

In summary, we have successfully fabricated ferroelectric BTO thin films on polycrystalline nickel substrates using PAD, with the design of a NiO_x buffer layer and a first annealing in a reducing environment. It is indicated that a proper treatment of a second annealing in oxygen is important to reduce the leakage current density and the dielectric loss. Leakage current mechanisms have been analyzed. It is suggested that the second annealing affects not only the interface barrier but also the bulk defect concentration, which could be attributed to the competition of the compensation of oxygen vacancies and the interdiffusion between BTO films and Ni substrates. Reduction of about two orders of magnitude in leakage current density and 47% in dielectric loss can be achieved in the BTO films with the optimized second annealing time. The successful fabrication of these ferroelectric thin films

by the PAD with two-step annealing technique provides a feasible way to develop various devices.

Acknowledgements

This work is supported by the National Basic Research Program of China (973 Program) under Grant No. 2015CB351905, the National Natural Science Foundation of China (Nos. 51372034, 11329402 and 51172036) and Guangdong Innovative Research Team Program (No. 201001D0104713329).

References

[1] J.F. Scott, Science 315 (2007) 954–959.
[2] R.A. Mckee, F.J. Walker, E.D. Specht, G.E. Jellison Jr., L.A. Boatners, J.H. Harding, Phys. Rev. Lett. 72 (1994) 2741–2744.
[3] N. Setter, Electroceramic-Based MEMS, fourth ed., Springer, New York, 2005.
[4] D.L. Polla, L.F. Francis, Annu. Rev. Mater. Sci. 28 (1998) 563–597.
[5] D.M. Gill, C.W. Conrad, G. Ford, B.W. Wessels, S.T. Ho, Appl. Phys. Lett. 71 (1997) 1783–1785.
[6] H. Yang, J. Miao, B. Chen, L. Zhao, B. Xu, X.L. Dong, L.X. Cao, X.G. Qiu, B.R. Zhao, Appl. Phys. Lett. 85 (2004) 4106–4108.
[7] B. Chen, H. Yang, J. Miao, L. Zhao, L.X. Cao, B. Xu, X.G. Qiu, B.R. Zhao, J. Appl. Phys. 97 (2005) 024106.
[8] S. Halder, T. Schneller, R. Meyer, R. Waser, J. Appl. Phys. 97 (2005) 114904.
[9] A.I. Kingon, S. Srinivasan, Nat. Mater. 4 (2005) 233–237.
[10] V. Sethi, G. Song, J. Vib. Control. 11 (2005) 671–684.
[11] J.T. Dawley, P.G. Clem, Appl. Phys. Lett. 81 (2002) 3028–3030.
[12] T. Dechakupt, G.Y. Yang, C.A. Randall, S. Trolier-McKinstry, I.M. Reaney, J. Am. Ceram. Soc. 91 (2008) 1845–1850.
[13] I. Bretos, T. Schneller, R. Waser, D.F. Hennings, S. Halder, F. Thomas, J. Am. Ceram. Soc. 93 (2010) 506–515.
[14] Z. Yuan, J. Liu, J. Weaver, C.L. Chen, J.C. Jiang, B. Lin, V. Giurgiutiu, A. Bhalla, R.Y. Guo, Appl. Phys. Lett. 90 (2007) 202901.
[15] J.C. Jiang, E.I. Meletis, Z. Yuan, J. Liu, J. Weaver, C.L. Chen, B. Lin, V. Giurgiutiu, R.Y. Guo, A.S. Bhalla, D. Liu, K.W. White, J. Nano Res. 1 (2008) 59–63.
[16] J. Shin, A. Goyal, S. Jesse, D.H. Kim, Appl. Phys. Lett. 94 (2009) 252903.
[17] L.J. Bao, J. Ryley, Z. Li, C. Wilker, L. Zhang, D. Reardon, R. Opila, J. Appl. Phys. 106 (2009) 114114.
[18] S.M. Aygun, P. Daniels, W. Borland, J.P. Maria, J. Appl. Phys. 103 (2008) 084123.
[19] R. Streubel, D. Köhler, R. Schäfer, L.M. Eng, Phys. Rev. B 87 (2013) 054410.
[20] W.Z. Liang, Y.D. Ji, T. Nan, J. Huang, H. Zeng, H. Du, C. Chen, Y. Lin, Chin. Phys. B 21 (2012) 067701.
[21] W.Z. Liang, Y.D. Ji, T. Nan, J. Huang, Z. Bi, H. Zeng, H. Du, C. Chen, Q. Jia, Y. Lin, ACS Appl. Mater. Interfaces 4 (2012) 2199–2203.
[22] W.Z. Liang, Z. Li, Z. Bi, T. Nan, H. Du, C. Nan, C. Chen, Q. Jia, Y. Lin, J. Mater. Chem. C 2 (2014) 708–714.
[23] Q.X. Jia, T.M. McCleskey, A.K. Burrell, Y. Lin, G.E. Collis, H. Wang, A.D.Q. Li, S.R. Foltyn, Nat. Mater. 3 (2004) 529–532.
[24] R. Meyer, R. Liedtke, R. Waser, Appl. Phys. Lett. 86 (2005) 112904.
[25] H. Yang, H. Wang, G.F. Zou, M. Jain, N.A. Suvorova, Appl. Phys. Lett. 93 (2008) 142904.
[26] H. Yang, Y.Q. Wang, H. Wang, Q.X. Jia, Appl. Phys. Lett. 96 (2010) 012909.
[27] Y. Podgorny, A. Sigov, A. Vishnevskiy, K. Vorotilov, Ferroelectrics 465 (2014) 28–35.
[28] R.K. Pan, T.J. Zhang, J.Z. Wang, Z.J. Ma, J.Y. Wang, D.F. Wang, J. Alloys Comp. 519 (2012) 140–143.
[29] C.A. Randall, R. Maier, W. Qu, K. Kobayashi, K. Morita, Y. Mizuno, N. Inoue, T. Oguni, J. Appl. Phys. 113 (2013) 014101.
[30] P.M. Raj, S. Xiang, M. Kumar, I.R. Abothu, J.H. Hwang, Y. Liu, H. Yamamoto, R. Tummala, J. Mater. Sci.: Mater. Electron. 23 (2012) 901–908.
[31] S. Zafar, R.E. Jones, B. Jiang, B. White, P. Chu, D. Taylor, S. Gillespie, Appl. Phys. Lett. 73 (1998) 175–177.
[32] J.S. Lee, Y. Li, Y. Lin, S.Y. Lee, Q.X. Jia, Appl. Phys. Lett. 84 (2004) 3825–3827.
[33] F.M. Pontes, E.R. Leite, E. Longo, J.A. Varela, E.B. Araujo, J.A. Eiras, Appl. Phys. Lett. 76 (2000) 2433–2435.
[34] K.T. Li, V.C. Lo, J. Appl. Phys. 97 (2005) 034107.
[35] X.D. Qi, J. Dho, R. Tomov, M.G. Blamire, J.L. MacManus-Driscoll, Appl. Phys. Lett. 86 (2005) 062903.
[36] I. Barin, Thermochemical Data of Pure Substances, third ed., Wiley-VCH Verlag GmbH, Weinheim, 1995.
[37] Y. Li, M. Gao, H. Du, Y. Zhang, Y. Lin, J. Chin. Ceram. Soc. 42 (2014) 1240–1246.
[38] S.T. Chang, J.Y. Lee, Appl. Phys. Lett. 80 (2002) 655–657.
[39] A.R. Chaudhuri, S.B. Krupanidhi, J. Appl. Phys. 98 (2005) 094112.
[40] L. Zhang, J. Zhai, W. Mo, X. Yao, Solid State Sci. 12 (2010) 509–514.
[41] A. Rose, Phys. Rev. 97 (1955) 1538–1544.